A Modelling-Mapping Approach for Fine-Scale Natural Ventilation Evaluation in High Density Cities

Chao Yuan[1, 2], Leslie Norford[3], Rex Britter [4], Edward Ng[5],

[1] Massachusetts Institute of Technology, 77 Mass. Ave, Cambridge, MA, US. yuanc@mit.edu
2 Singapore University of Technology and Design, 8 Somapah Rd, Singapore.
3 Massachusetts Institute of Technology, 77 Mass. Ave, Cambridge, MA, US. lnorford@mit.edu
4 Massachusetts Institute of Technology, 77 Mass. Ave, Cambridge, MA, US. rexb@mit.edu
5 The Chinese University of Hong Kong, Shatin, Hong Kong. edwardng@cuhk.edu.hk

ABSTRACT

This study develops an approach to model the pedestrian-level wind speed at high spatial resolution within urban areas. The aerodynamic properties of urban areas are a necessary component in current urban planning and design. However current numerical modelling methods, such as Computational Fluid Dynamics (CFD), cannot balance modelling cost with result accuracy to satisfy the requirements of urban design at the neighborhood scale. Alternatively, current morphological models, algorithms that correlate urban geometries with aerodynamic properties, are inexpensive but can only provide results with low spatial resolution. This study describes the balance between the momentum transfer and drag force in both an averaged sense over an area and a moving air particle to extend conventional frontal area density (λ_f) to a point-specific parameter (λ_{f_point}). Through correlation with data from wind tunnel experiments, λ_{f_point} is determined to be a good index to assess the pedestrian-level wind speed at a test point with multiple input wind directions. Regression equations are developed to map the pedestrian-level wind environment at 1m × 1m pixel resolution. This modelling-mapping approach requires less computational time and support technology than CFD simulations. Meanwhile, from a practical point of view, the modelling method provides accurate results at high resolution. Therefore, the modelling results of the urban wind environment can be well integrated into the neighborhood-scale design. Using this approach, urban planners can estimate the neighborhood-scale pedestrian-level wind speed and optimize proposed planning at the onset of the planning procedure.

Keywords: Fine-scale wind estimation, Momentum transfer, Urban design and planning

1. INTRODUCTION

Due to rapid urbanization and depletion of natural resources, high-density urban living that better use natural resources is an inevitable growing trend. However, closely packed high-rise buildings often result in stagnant airflow in high-density urban areas, which has been associated with increased exposure to ambient air pollution and outdoor thermal discomfort (Cheng et al., 2011; Y. Tominaga & Stathopoulos, 2009). Therefore, improvement of the urban environment using wind flow and dispersion information is among the fundamental tasks of high-density urban planning. In this study, we aimed to develop a fine-scale morphological modelling-mapping approach to provide pedestrian-level wind information between buildings, which could enable more efficient decision-making in urban planning and design. This approach not only could avoid high computational costs as opposed to what Computational Fluid Dynamics (CFD) simulation requires(Yoshihide Tominaga et al., 2008), it could also increase the resolution of the wind environment map to several meters, compared with the hundred meters resolution in the conventional morphological models (Gál & Unger, 2009; Ng et al., 2011; Wong et al., 2010). Consequently, our new approach could bridge the gap between the current modelling methods and requirements of practical planning and design.

2. LITERATURE REVIEW

Using a combination of numerical models in different scales, such as Weather Research and Forecasting (WRF) and Computational Fluid Dynamics (CFD), one can describe the urban air flow features and study outdoor urban wind environment (Bentham and Britter, 2003). However, numerical

models require high computational cost, therefore it is not suitable for the quick design and planning processes. Ng et al. (2011) suggests that semi-empirical morphological modelling (Grimmond & Oke, 1999) may be a more practical tool. Semi-empirical morphological methods were developed by correlating geometric indices, such as frontal area density (the ratio between frontal area and site area, λ_f), and the site coverage ratio (the ratio between built area and site area, λ_p), with experimental wind data, so that the algorithms of geometric indices can be used to estimate the wind environment. By using the morphological models, the complicated calculations of fluid mechanics can be avoided, thereby significantly reducing the computational costs.

Bentham and Britter (2003) developed a practical and comprehensive morphological model to estimate the uniform wind speed (U_c) at the urban canopy layer. The experiment data of U_c normalized by frictional velocity u_* is well related with modelling result, as shown in Figure 1. We plotted Hong Kong data (Ng et al., 2011) in Figure 1, using the local values of λ_f and U_c/u_* which was estimated by the wind speed data from wind tunnel experiment (i.e. λ_f =1.4 and VR =0.15). The result indicated that Bentham and Britter's model is still valid at the high density areas with λ_f equal to 1.4. By comparing with previous studies (MacDonald, et al., 1998; Raupach, 1992; Zhu, et al., 1998; Haven et al., 1996; Petersen and Ratcliff, 1989; Cheng and Castro, 2002), Figure 1 also comprehensively shows the low wind speed at the urban canopy layer and high density in this study.

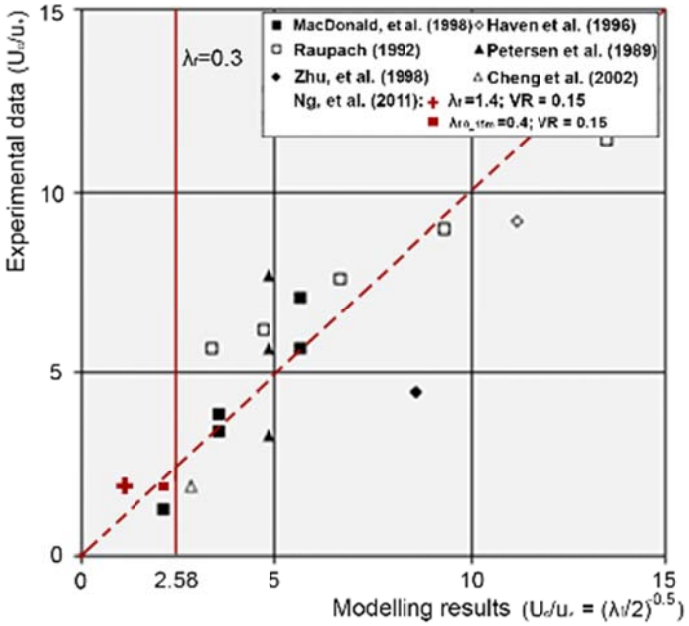

Figure 1: Comparison of morphological modelling results for U_c with experiment data (Bentham and Britter, 2003, edited by authors). The results for the high density area are included as red plots.

However, the conventional morphological models are invalid to estimate the pedestrian-level wind speed at the urban canopy layer when λ_f is larger than 0.3-0.4 (Grimmond and Oke, 1999). As shown in Figure 1, when λ_f exceeds 0.3, i.e. the modelling result of U_c/u_* is less than 2.58, the significant increase of λ_f only associates with a small decrease of U_c, because that the buildings interfere with each other and the wind profile in the street canyon is not logarithmic (MacDonald et al., 1998). Therefore, a new parameter is needed to estimate the pedestrian-level wind speed at urban areas with the high density. Second, the conventional models are not suitable for estimating wind speed at the neighborhood-scale, i.e., the order of 1 km horizontal spacing (Belcher et al., 2003). Since these models are developed based on the balance between spatially averaged momentum flux and drag force, they can only provide spatially averaged wind information, with resolutions ranging from several hundred to thousand meters. However, the mean wind speed between buildings significantly varies at the neighborhood scale due to spatial heterogeneity, and is important for evaluations of outdoor thermal

comfort and air quality (Coceal & Belcher, 2005). As a result, a more refined morphological model is needed for applications at the neighborhood scale.

3. MODEL DEVELOPMENT

3.1 Relating λ_f to the pedestrian-level wind speed at high density areas

Given the steady and uniform air flow, there is a balance between the drag force of buildings on the air flow and turbulent momentum transfer downward from above as:

$$\rho D = -\rho \frac{\partial}{\partial z}\langle \overline{u'w'} \rangle \quad (1)$$

where ρD is the canopy drag force, the body force per unit volume on the spatially averaged flow, and $\rho\langle \overline{u'w'} \rangle$ is the momentum flux caused by turbulent mixing. The momentum flux by turbulent mixing can be considered as shear stress (τ_w) that is given by Zhang et al. (2014):

$$\frac{\partial}{\partial z}\tau_w = -\rho \frac{\partial}{\partial z}\langle \overline{u'w'} \rangle \quad (2)$$

The total canopy drag force (ρD) is given by (Bentham & Britter, 2003):T

$$\rho D = \frac{1}{2}\rho U_c^2 \frac{\sum_{obstacle}(C_D A_{front})}{hA_{site}(1-\lambda_p)} \quad (3)$$

where A_{front} is the frontal area, U_c is the averaged wind speed in the canopy layer, and C_D is the drag coefficient. The air volume is given by $hA_{site}(1-\lambda_p)$, where A_{site} is the site area, h is the canopy height, and λ_p is the site coverage ratio. Substituting the expression for $\rho \frac{\partial}{\partial z}\langle \overline{u'w'} \rangle$ (equation 2) and ρD (equation 3) into equation (1) yields another statement of the balance between canopy drag and vertical transfer of horizontal momentum in height z:

$$\frac{\partial}{\partial z}\tau_w = \frac{1}{2}\rho U_{(z)}^2 \sum_{obstacle}(C_{D(z)} \frac{dA_{front}}{dz})/A_{site}(1-\lambda_p) \quad (4)$$

It should be noted that the right side of equation (4) is the sectional drag acting only at height z, where U_z is the wind speed at height z and $C_{D(z)}$ is the sectional drag coefficient (Coceal & Belcher, 2004). Cheng and Castro (2002) found that $C_{D(z)}$ is equal to 2.0 near the top because air can flow over and around roughness elements at the top, and $C_{D(z)}$ increases to 3.0 over the remaining depth, since the air only can flow around roughness elements in the remaining depth, i.e. the sectional drag is enhanced. Given the deep street canyon, we set $C_{D(z)}$ equal to 3.0 in this study. Consequently, the wind speed (U_i) in the i[th] layer of the street canyon is given by re-arranging equation (4) as:

$$U_i = \left(\frac{\tau_{w,i}}{3\rho} \cdot \frac{2(1-\lambda_p)}{\lambda_{f,i}}\right)^{0.5}, \ (\text{where } \lambda_{f,i} = \frac{A_{front,i}}{A_{site}}) \quad (5)$$

Bentham and Britter (2003) ignored the vertical variation of $\tau_{w,i}$ by using the equivalent surface shear stress (τ_w) and considered C_D is equal to 1.0. They treated the air volume between two rows of buildings as the control volume, therefore λ_p in equation 5 is equal to 0. Consequently, they provided a practical method to estimate the averaged velocity in the urban canopy U_c as:

$$\frac{U_C}{u_*} = \left(\frac{\lambda_f}{2}\right)^{-0.5}, \ (\text{where } u_* \text{ is equal to } \left(\frac{\tau_w}{\rho}\right)^{0.5}) \quad (6)$$

Equation (5) relates the wind speed (U_i) to the corresponding values of $\lambda_{f,i}$, ignoring the vertical variation of $\tau_{w,i}$ as Bentham and Britter (2003) did. This understanding is consistent with MacDonald et al. (1998): the frontal area density above the displacement height (z_d), λ_f^*, can better estimate the wind profile than λ_f; on the other hand, the near-ground wind speed is postulated to depend on λ_f', the frontal area density below z_d, instead of λ_f^*. Ng et al. (2011) defined the podium layer (0m - 15m) in Hong Kong due to the podium morphological characteristic as shown in Figure 2, and considered that

the air is impeded at the podium layer as much as if it is under z_d. The wind velocity ratio (VR) is well correlated to λ_f', which is represented by $\lambda_{f\ (0-15\ m)}$, rather than conventional λ_f, as shown in Figure 3. It should be mentioned that the averaged results for the conventional λ_f at Hong Kong (Ng, et al., 2011), λ_f = 1.4 and VR = 0.15, are consistent with the Bentham and Britter (2003)'s modelling result, as shown in Figure 1. Since we chose Hong Kong as the target city and focus on the estimation of pedestrian-level wind speed, we applied λ_f' calculated from 0m to 15m in this study.

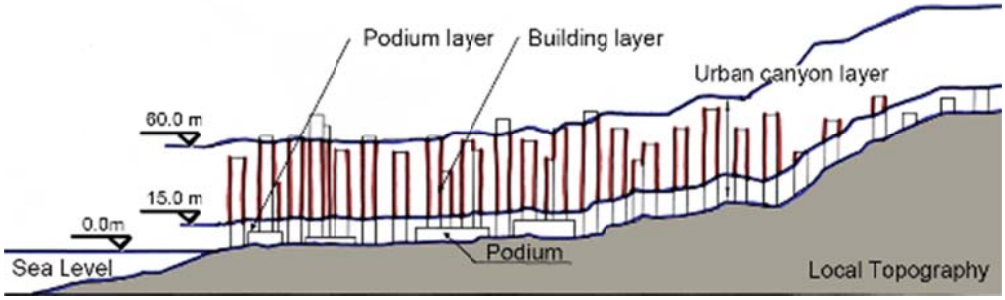

Figure 2: Conceptual representation of the sectional frontal area density, i.e. $\lambda_{f\ (0-15\ m)}$ which represents λ_f' in this study (Ng, et. al., 2011).

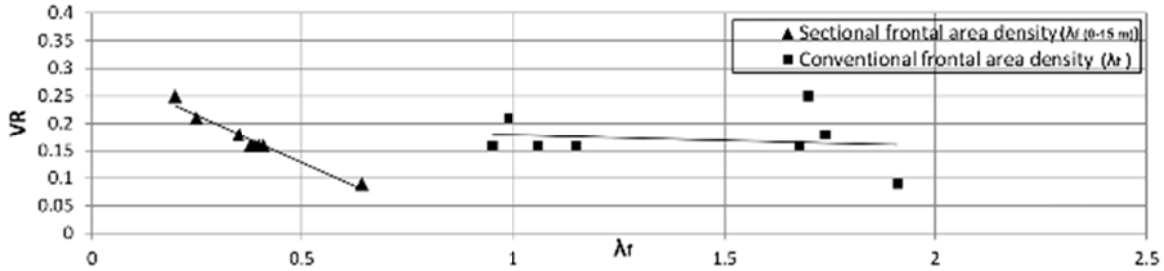

Figure 3: Comparison of conventional and sectional λ_f with experiment data. The VR and λ_f are the spatially averaged results in 300m × 300m grid (Ng, et al, 2011, edited by authors).

3.2 Adjustment of λ_f' to the fine-scale wind estimation

We estimated the fine-scale wind speed by adjusting the morphological index λ_f' using the distance from buildings to target points. As mentioned in section 3.1, the momentum transfer and drag force balance is spatially averaged for the whole control volume, and each building, i.e. roughness element, is treated equally to calculate the spatially averaged indices. Here, we illustrated how air flows through urban areas by describing the momentum transfer and drag force balance in a moving air particle. The air particle is impeded by the drag force of buildings, and is accelerated by the downward transfer of horizontal momentum. This means that the air particle will stop without vertical transfer of horizontal momentum (Belcher et al., 2003; Hall, 2010). The speed of the air particle can be recovered after traveling further away from the building. It indicates that, when the wind speed at test points is affected by the surrounding area, the effects of frontal area units are different, given that the distances from the target point to individual frontal area units are different. Consequently, we created a distance index (L) and calculated the point-specific frontal area density (λ_{f_point}) by adjusting λ_f' using the distance index (L). This adjustment of calculation means that $\lambda_{\text{f-point}}$ is not only spatially and annually averaged but also point-specific. As shown in Figure 4, frontal area pixels in Δz (0m -15m) ($A_{\Delta z,i}$), weighted by the distance coefficient (l) and annual wind frequency (P_i) in the i[th] wind direction, were added up and normalized by the scanned area to calculate the point-specific frontal area density (λ_{f_point}) as:

$$\lambda_{\text{f\_point}} = \frac{\iint_D l_{x,y}^{\xi}(A_{\Delta z,x,y}/A_t)\,dx\,dy}{A_t},\ D = \{x^2 + y^2 \le r^2\} \quad (7)$$

$$A_{\Delta z,x,y} = \sum_1^{i=16} A_{\Delta z,i} p_i \quad (8)$$

$$l_{x,y} = \frac{r-L}{r} \quad (9)$$

$$A_t = \pi \cdot r^2 \quad (10)$$

where $A_{\Delta z,x,y}$ is the wind frequency-weighted frontal area at the pixel (*x*, *y*), in which *x* and *y* are the coordinates (the test point is the origin of the coordinate), Δz is from 0-15 m (Ng et al., 2011), and $l_{x,y}$ is the distance coefficient. The A_t is the scanned area and *r* is the scan radius (200 m) (Ng et al., 2011), as shown in Figure 4. Belcher et al. (2003) indicates that the increase of the mean wind speed is not linear when the air particle gets further away from the roughness elements. Therefore, an exponent c, 2.0, is used to adjust $l_{x,y}$. As indicated in Table 1, the modelling results with the exponent c=2.0 fit the experimental data better than the one with the exponent c=1.0.

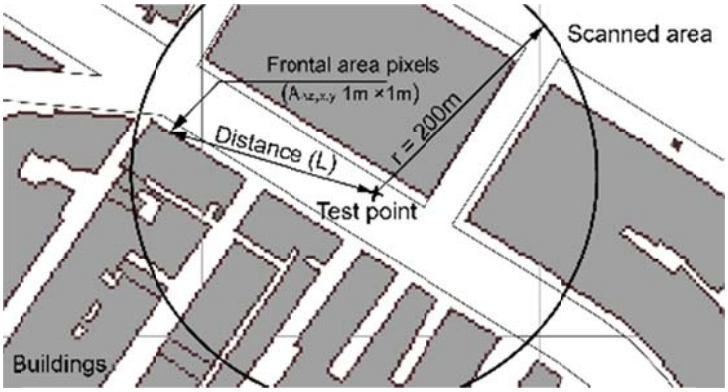

Figure 4: Schematic illustration of λ_{f_point} calculation method. Test point, scanned area (A_t), radius (*r*), distance (L), frontal area units (red pixels) at the boundaries of buildings are presented.

4. MODELLING TEST

We correlated the wind tunnel data with the point-specific index (λ_{f_point}) to test the model performance. The wind tnnel experiment was carried out at six locations, as shown in Figure 5. Three of them, i.e. Mong Kok, Sheung Wan, and Causeway Bay, are located at the metropolitan area, and the remainder, Tuen Mun, Sha Tin, and Tseung Kwan O, are located in new town areas. The data from metropolitan areas are used to develop the linear regression model, and the data from new town areas are used to test the performance of the linear regression model at the urban areas with different densities.

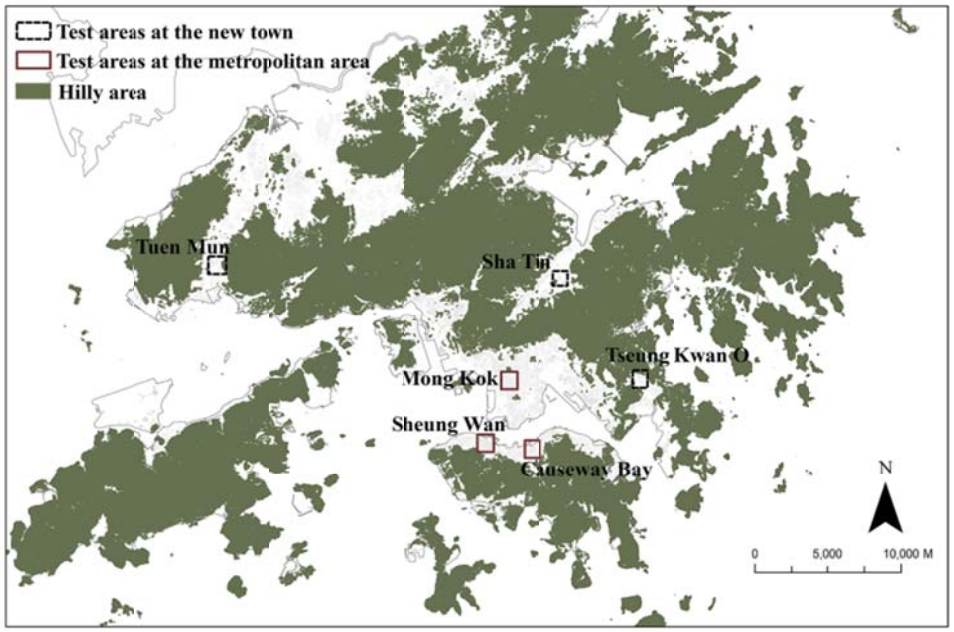

Figure 5: Six test locations where the wind tunnel data was collected: black dash boxes: new town areas; red solid boxes: metropolitan areas.

4.1 Sensitivity of pedestrian-level wind speed on λ_{f_point}

As shown in Figure 6, each location at metropolitan areas has two zones (Zone a and Zone b) and test points are evenly distributed to collect the overall wind VR, as:

$$VR = \sum_{i=1}^{16} P_i \cdot VR_{500,i} \quad (11)$$

where $VR_{500,i}$ represents the directional wind velocity ratio between wind speeds at the pedestrian level and 500 m above the ground (reference height). Results of the regression analyses were plotted in Figure 7 and summarized in Table 1. In general, the point-specific λ_{f_point} is negatively associated with wind VR. In other words, the closer surrounding roughness elements to the test point, the more the air flow would be impeded, and the slower the pedestrian-level wind speed at a particular point.

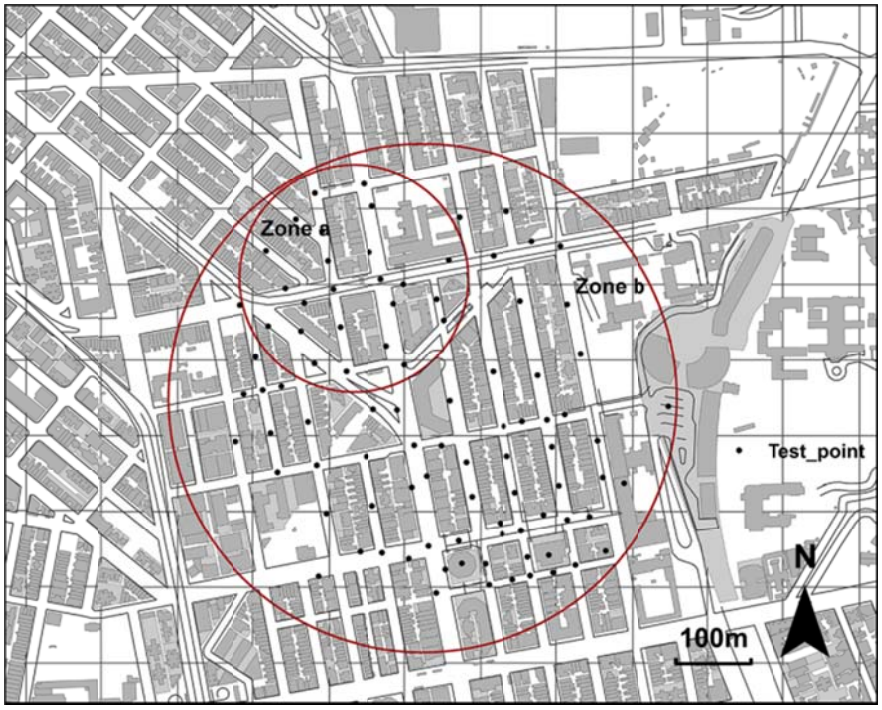

Figure 6: Test points in test locations (Mong Kok as the example). Every test location includes two zones (Zone a and Zone b).

The statistical analysis indicates an acceptable modelling-mapping method from the practical planning and design perspective, i.e. the urban planners and architects can use λ_{f_point} to well predict the VR. The values of R^2 ranged from 0.40 to 0.62. The values of confidence intervals (CI) and standard error (SE) are one order of magnitude smaller than the corresponding predicted values. As shown in Figures 8a and 8b, the 95% confidence intervals (CI) of the slopes of the regression model for irregular and regular street grid are -1.66±0.14 and -3.83±0.56 respectively. The standard error (SE) of predicted VR at test zones is about 0.04. Furthermore, using the annually averaged wind speed at the reference height (500 m above the ground) at the test locations, 6.67 m/s, which is an MM5 modeling result (Yim, et al., 2007), we also calculated the SE of predicted pedestrian-level wind speed that is about 0.27 m/s. The sensitivity of physiological equivalent temperature (PET) on the change of wind speed at this range is low (more about the sensitivity of PET on the wind speed is in Section 5). Therefore, it is considered that the accuracy of the modelling result is acceptable to the purpose of urban planning and design.

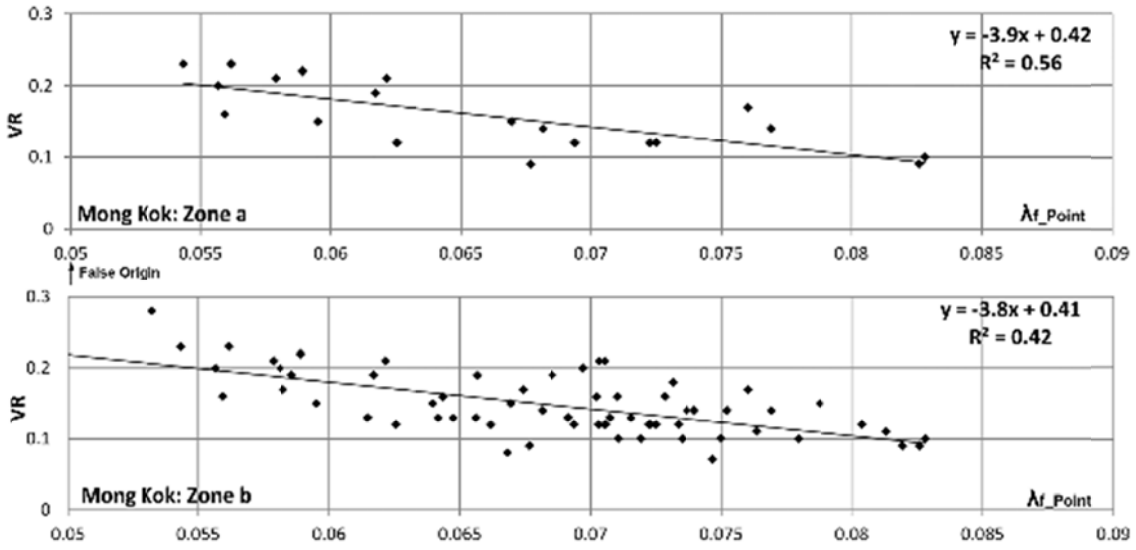

Figure 7a: Linear regression analysis at Mong Kok: Zone a and Zone b.

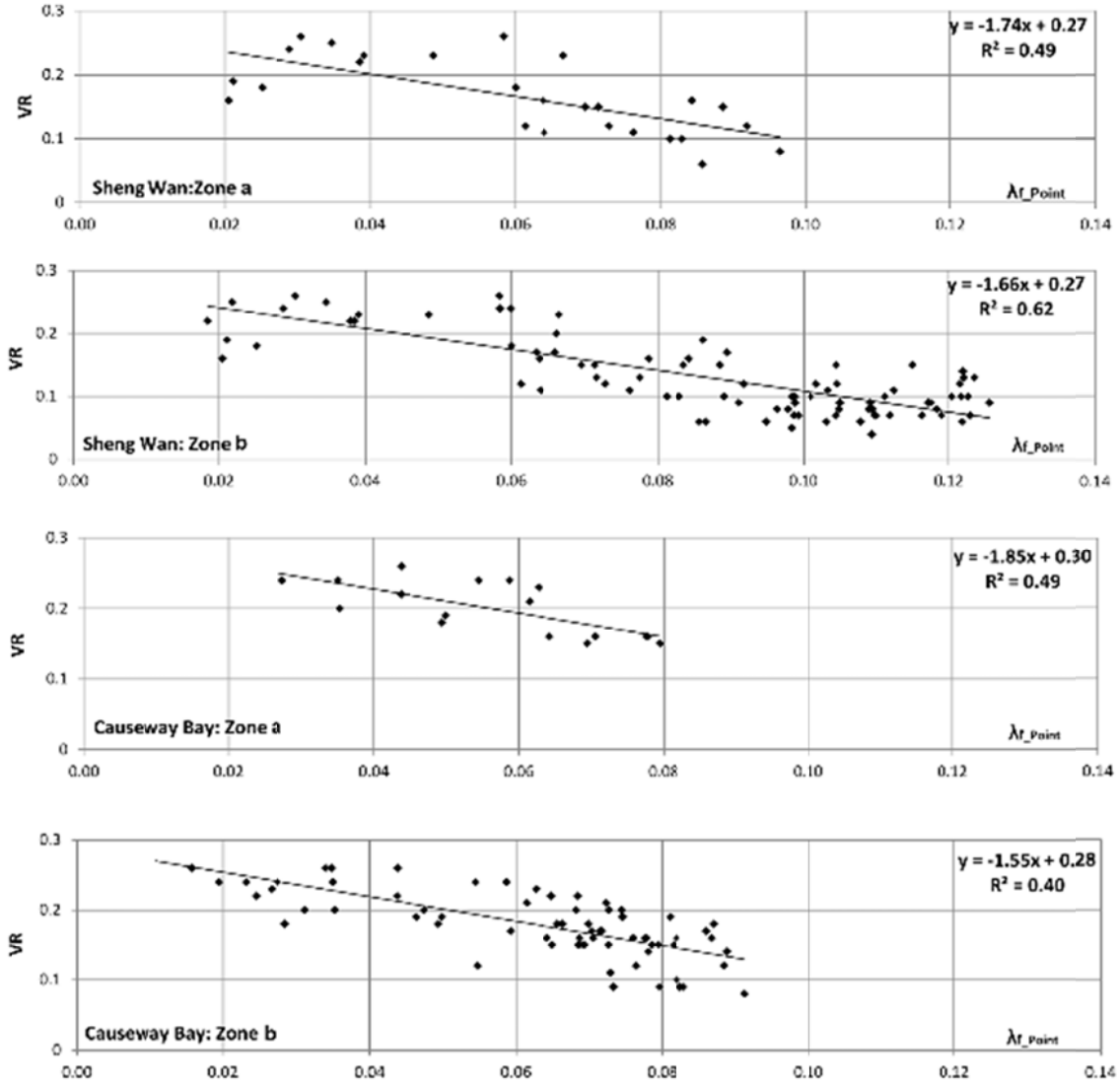

Figure 7b: Linear regression analysis at Sheung Wan and Causeway Bay: Zone a and Zone b.

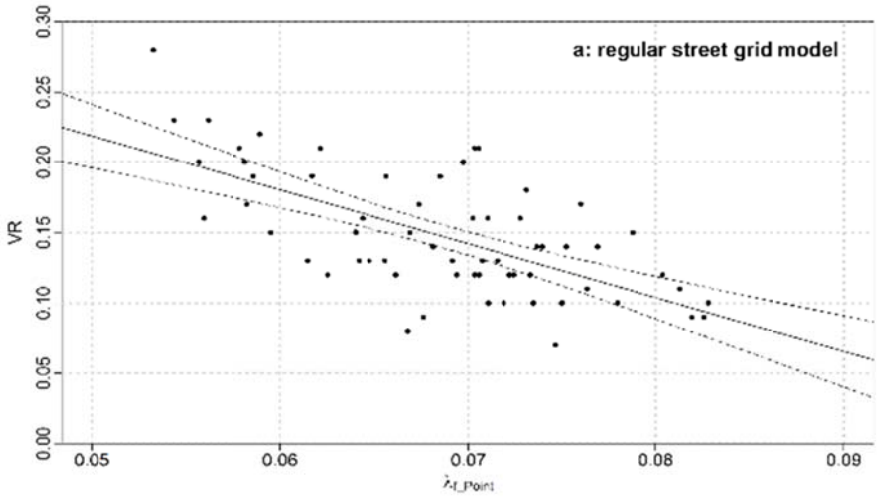

Figure 8a: 95% confidence interval for regression analysis for the regular street grid. The slope is equal to -1.66±0.14, taking Mong Kok (Zone b) as example.

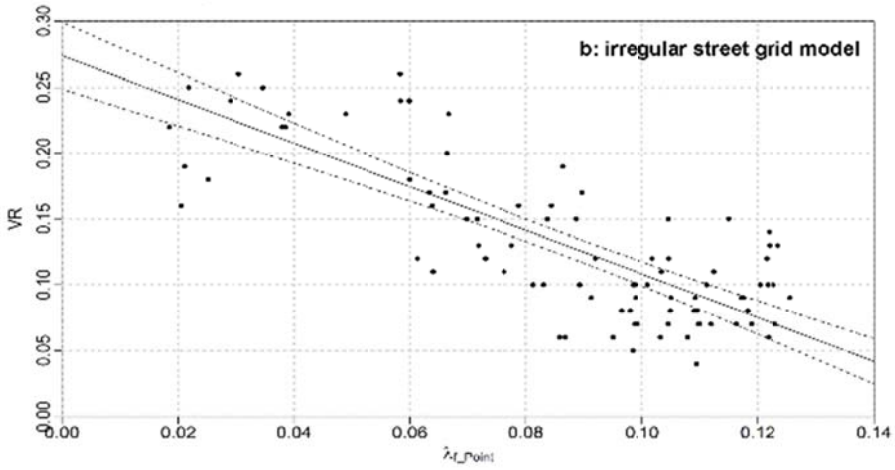

Figure 8b: 95% confidence interval for regression analysis for the irregular street grid. The slope is equal to -3.83±0.56, taking Sheung Wan (Zone b) as example.

Table 1 shows that the slopes between street grids (regular versus irregular) are different. The slope for Mong Kok (-3.9) is significantly different from those for Sheung Wan and Causeway Bay (-1.7). The incoming air in areas with regular street grids might encounter strong resistance, and the wind speed is particularly small at streets that are perpendicular to the wind direction, given that air flow at those streets is only driven by the limited horizontal momentum transferred from the street that is aligned with the wind direction. In contrast, incoming air can easily flow around a building block in areas with irregular street grids, driven by the horizontal momentum. Thus, the same frontal area can impede more air flow in regular street grid than in irregular street grid, which explains the different coefficients and intercepts in urban areas with different street grids in Table 1. However, values of slopes in Table 1 also show that the slopes for different test zones within the same street grid are similar. Therefore, it is possible to develop the general regression equation to predict VR by using λ_{f_point} for each type of street grids as:

i) for districts with regular street grids (main streets perpendicular with each other, as shown in Figure 6):
$$VR = -3.9\lambda_{\mathrm{f\_point}} + 0.41 \quad (12)$$

ii) for districts with irregular street grids, as shown in Figure 11:
$$VR = -1.7\lambda_{\mathrm{f\_point}} + 0.28 \quad (13)$$

Table 1: Slope Coefficient, Intercept, and Standard Error in regression equations for different districts. The result of sensitivity test of exponent c was also presented.

Districts	Zones	R^2 (exponent c=1.0)	R^2 (exponent c=2.0)	Slope Coefficient	Intercept	SE of predicted VR	SE of predicted U_p (m/s)
Mong Kok (Grid plan)	Zone a	0.52	0.56	-3.9	0.4	0.03	0.20
	Zone b	0.14	0.42	-3.8	0.4	0.04	0.27
Sheung Wan (Irregular street grid)	Zone a	0.35	0.49	-1.7	0.3	0.05	0.33
	Zone b	0.57	0.62	-1.7	0.3	0.04	0.27
Causeway Bay (Irregular street grid)	Zone a	0.47	0.49	-1.9	0.3	0.03	0.20
	Zone b	0.40	0.40	-1.6	0.3	0.04	0.27

4.2 Performance of regression models at urban areas with lower density

In this section, we tested the performance of the regression model at new town areas with lower densities, as shown in Figure 5. It is clear that the urban density of new town areas (Figures 9a, 9b, and 9c) is much lower than at metropolitan areas (Figures 9d, 9e, and 9f).

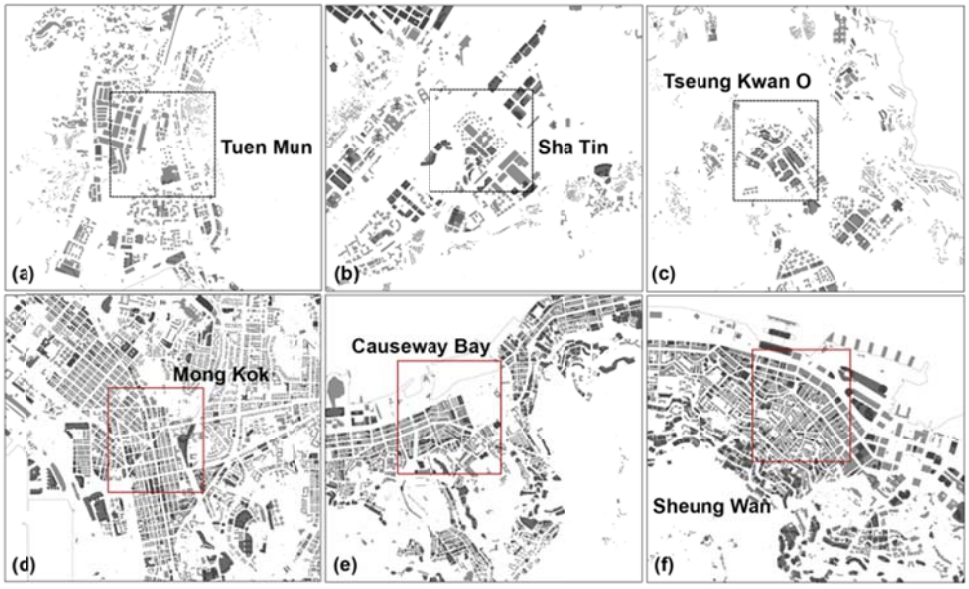

Figure 9: Different densities between new town areas (a, b, c) and metropolitan areas (d, e, f). The calculating areas were also highlighted.

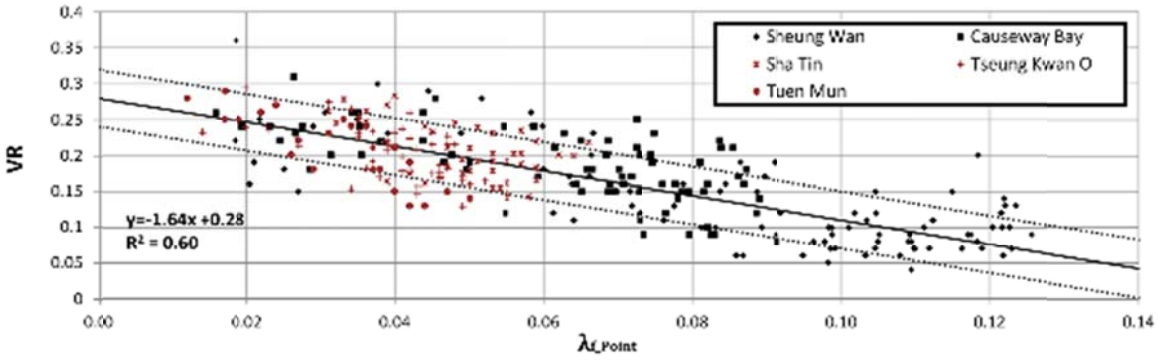

Figure 10: Sensitivity analysis of new morphological model to determine pedestrian-level wind speed normalized by wind speed at the reference height. Black plots are for the urban areas with high density and the red plots are for the urban areas with low density. The standard error is 0.04.

The VR and λ_{f_point} from these three new town areas were plotted in Figure 10 together with the data from the metropolitan areas. It indicates that the linear relations for urban areas with high and low density are same, i.e. the same linear equation could be used at the different urban areas, even though the range of λ_{f_point} is much smaller at the urban areas with the low density.

5. MAPPING THE WIND ENVIRONMENT IN THE NEIBORHOOD SCALE

Based on the above analysis, we applied λ_{f_point} to map the pedestrian-level wind speed in the neighborhood scale. As shown in Figure 11, we first used equations 7 – 10 to calculate λ_{f_point} on a pixel by pixel (1 m × 1 m) basis of all non-built-up locations in the target area, by applying a self-developed program, which is embedded as a Visual Basic for Applications (VBA) script in the ArcGIS System. Second, we extended the λ_{f_point} map to the overall wind VR map, using the regression either equations 12 or 13, as shown in Figure 11. Both λ_{f_point} and VR in Figure 11 quantitatively present the urban permeability at the target area. This map reflects a common perception of the wind environment. Specifically, urban permeability is the highest (green area) in coastal areas (VR larger than 0.2). The wind permeability significantly decreases toward deep urban areas (VR smaller than 0.1) in prevailing wind directions (red area), given that the model took the wind frequency into account.

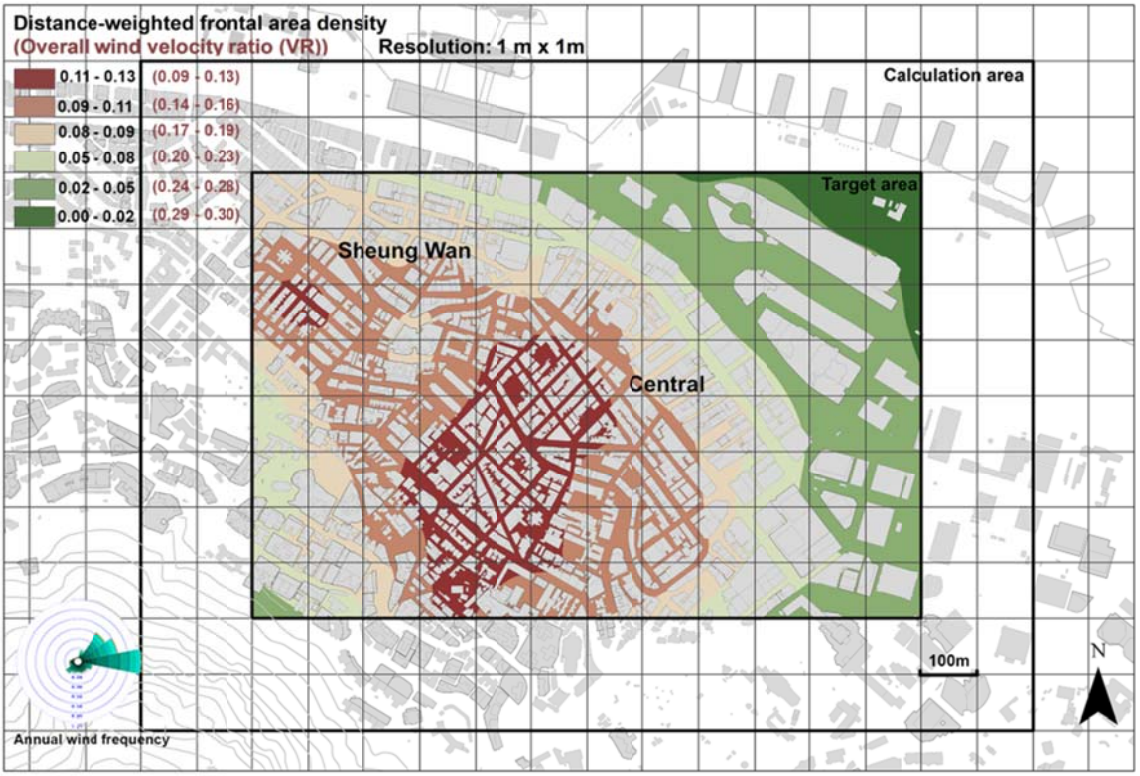

Figure 11: Map of $\lambda_{f\text{-point}}$ and estimated overall wind velocity ratio (VR) for Sheung Wan and Central, which represent the annually averaged wind permeability. Wind permeability in coastal areas is high (green area) and significantly decreases toward deep urban areas in prevailing wind directions (red area).

We also calculated and mapped annually averaged pedestrian-level wind speed (U_p) based on the definition of wind VR (equation 11) by multiplying VR by U_{500} (annually averaged wind speed) at the reference height, 6.67m/s at Sheung Wan and Central. Using the wind classification based on physiological equivalent temperature (PET) (Cheng et al., 2011), the neighborhood wind speed field can be classified as Class 1 (Poor, <0.6 m/s), Class 2 (Low, 0.6–1.0 m/s), Class 3 (Satisfactory, 1.0 m/s – 1.3 m/s) and Class 4 (Good, >1.3 m/s). The pedestrian-level wind speed map with the classification is shown in Figure 12.

Figure 12: Pedestrian-level wind speed map, which was classified as Class 1 (Poor, <0.6 m/s), Class 2 (Low, 0.6 m/s -1.0 m/s), Class 3 (Satisfactory, 1.0–1.3 m/s), and Class 4 (Good, > 1.3 m/s).

6. IMPLEMENTATION

The new modelling and mapping method, with the low computational cost, accurate and high resolution modelling results, is considered as a practical tool for the urban planning and design in the neighborhood scale. Compared to the few hours of processing time needed for our proposed modelling method, it would take the CFD simulation or wind tunnel experiment several months to obtain a similar time averaged result (e.g., the annually-averaged wind environment in Figures 11 and 12). Also, the new modelling–mapping approach enables urban planners and designers to model and evaluate the wind environment by themselves. It should be noticed that the planners and designers should take into account the entire modelling results, rather than evaluating the values by pixels. For important projects with higher requirement for accuracy, CFD simulation or wind tunnel experiment is still required.

Taking Sheung Wan and Central in Hong Kong as an example, Ng et al. (2011) has shown that the wind permeability in these two areas is low. Although useful in master planning, such information is not fine enough in spatial resolution for district planning to improve the local wind environment. The new approach produces a pedestrian-level wind speed map (Figure 12) that provides fine-scale wind information (i.e. wind speed between buildings), and bridges the gap between master planning and district planning. As shown in Figure 12, compact building groups could impede air flow in the purple zone (Class 1: Poor, <0.6m/s), which has been associated with both outdoor thermal discomfort and poor air pollution dispersion. The wind environment at the yellow zone (Class 2: Low, 0.6 m/s – 1.0 m/s) is better than the one at the purple zone, but the outdoor thermal comfort and air quality remain two major concerns because the wind speed is still low. In contrast, the wind speed in the light green zone is satisfactory (Class 3: Satisfactory, 1.0 m/s – 1.3 m/s), which reflects better natural ventilation performance and air quality. The dark green zone (Class 4: Good, > 1.3 m/s), mostly located at the waterfront area with the lowest urban density, has the highest urban permeability.

Based on the above evaluation, urban planning and design strategies can be tailored to address specific wind environment issues at different zones. New development projects should not be allowed at the purple zone, and should be strictly controlled at the yellow zone with the detailed study of AVA evaluation. Given the low air pollutant dispersion in the purple and yellow zones, planners should not arrange additional bus stops, terminus, heavy traffic roads, or other land use with pollutant sources at these zones to avoid trapping the emitted air pollutant. On the other hand, new projects should be developed in the light green zone with cautions to avoid worsening the existing good wind environment. The public water front parks can be arranged at the dark green zone, given the good air quality and the outdoor thermal comfort. New bus stops, terminus, and other traffic facilities can be planned at this zone because the traffic -related air pollutant can be quickly dispersed.

7. Conclusion and Future Work

Upon broadly discussing the aerodynamic properties of urban areas and the corresponding planning principles, we developed a modelling–mapping approach to estimate the pedestrian-level wind speed in the neighborhood scale. High spatial resolution modelling results and low computational cost are two attractive features of this new approach. The key findings from this study are as following:

- Given the balance between vertical flux of horizontal momentum and horizontal drag force in the street canyon layer by layer, we used the sectional frontal area density (λ_f') below z_d to estimate the pedestrian level wind speed, particularly in the high density urban areas where the high buildings interfere with each other.
- We developed λ_{f_point} to estimate the effect of the neighborhood wind permeability on a particular point. We adjusted λ_f' by discussing the momentum transfer balance in a moving air particle. The distance index (L) is included into the morphological model to investigate the different effect of individual building on the wind speed at the target point.
- We tested the accuracy of the new morphological model using statistical analysis, and develop two regression equations to form a semi-empirical assessment tool to evaluate the pedestrian-level wind environment. The performance of this new tool was quantified by 95% confidence interval and standard error. The accuracy of the modelling results is acceptable for the urban design purpose at both high and low density urban areas.
- We discussed the different effects of regular and irregular street grids on the pedestrian-level wind speed, which are caused by different horizontal momentum transfer processes. In the regular street, air flow at the streets perpendicular to the wind direction is only driven by the limited horizontal momentum transferred from the street that is aligned with the wind direction.
- We applied the new method to two case studies at Hong Kong to illustrate how the modelling results could be use in the planning and design practice for better evidence-based decision making at the early stage of city planning.

References:

Belcher, S. E., Jerram, N., & Hunt, J. C. R. (2003). Adjustment of a turbulent boundary layer to a canopy of roughness elements. *Journal of Fluid Mechanics, 488*, 369-398.

Bentham, T., & Britter, R. (2003). Spatially averaged flow within obstacle arrays. *Atmospheric Environment, 37*(15), 2037-2043.

Cheng, V., Ng, E., Chan, C., & Givoni, B. (2011). Outdoor thermal comfort study in a subtropical climate: a longitudinal study based in Hong Kong. *International Journal of Biometeorology, 56 (1),43-56.*

Coceal, O., & Belcher, S. E. (2004). A canopy model of mean winds through urban areas. *Quarterly Journal of the Royal Meteorological Society, 130* (599), 1349-1372.

Coceal, O., & Belcher, S. E. (2005). Mean winds through an inhomogeneous urban canopy. *Boundary-Layer Meteorology, 115*(1), 47-68.

Gál, T., & Unger, J. (2009). Detection of ventilation paths using high-resolution roughness parameter mapping in a large urban area. *Building and Environment, 44*(1), 198-206.

Grimmond, C. S. B., & Oke, T. R. (1999). Aerodynamic properties of urban areas derived from analysis of surface form. *Journal of applied meteorology, 38*, 1262-1292.

Hall, C. T. (2010). *Predicting velocities and turbulent exchange in isolated street canyons and at a neighborhood scale.* Master of Science, Massachusetts Insititute of Technology, Cambridge, US.

MacDonald, R. W., Griffiths, R. F., & Hall, D. J. (1998). An improved method for the estimation of surface roughness of obstacle arrays. *Atmospheric Environment, 32*(11), 1857-1864.

Ng, E., Yuan, C., Chen, L., Ren, C., & Fung, J. C. H. (2011). Improving the wind environment in high-density cities by understanding urban morphology and surface roughness: a study in Hong Kong. *Landscape and Urban planning, 101*(1), 59-74.

Tominaga, Y., Mochida, A., Yoshie, R., Kataoka, H., Nozu, T., Yoshikawa, M., & Shirasawa, T. (2008). AIJ guidelines for practical applications of CFD to pedestrian wind environment around buildings. *Journal of Wind Engineering and Industrial Aerodynamics, 96*, 1749–1761.

Tominaga, Y., & Stathopoulos, T. (2009). Numerical simulation of dispersion around an isolated cubic building: Comparison of various types of k-epsilon models. *Atmospheric Environment, 43*(20), 3200-3210.

Wong, M. S., Nichol, J. E., To, P. H., & Wang, J. (2010). A simple method for designation of urban ventilation corridors and its application to urban heat island analysis. *Building and Environment, 45*(8), 1880-1889.

Zhang, Z. G., Chen, J. F., Yue, D. T., Yang, G. G., Ye, S., He, C. R., . . . Huang, N. B. (2014). Three-Dimensional CFD Modeling of Transport Phenomena in a Cross-Flow Anode-Supported Planar SOFC. *Energies, 7*(1), 80-98.